Journal of Solid State Chemistry **153,** 231–236 (2000)
doi:10.1006/jssc.2000.8746, available online at http://www.idealibrary.com on IDEAL®

Synthesis, Stoichiometry, and Electrical Transport Properties of $(Cd_{1-x}Mn_x)Mn_2O_4$

Paolo Ghigna,[1] Giovanni Battista Barbi, Gaetano Chiodelli, Giorgio Spinolo, Lorenzo Malavasi, and Giorgio Flor

INSTM, C.S.T.E./CNR, and Dipartimento di Chimica Fisica, Università di Pavia, Viale Taramelli 16, I 27100-Pavia, Italy

Received December 15, 1999; in revised form April 12, 2000; accepted April 20, 2000; published online July 17, 2000

This paper describes the synthesis and discusses the thermal stability, oxygen and cation stoichiometry, and electrical transport properties of Cd/Mn spinel materials. It has been found that an effective synthesis can be obtained by reacting in the solid state CdO and Mn_2O_3 in a closed quartz ampoule at 800°C. By following this synthetic procedure it was possible to prepare materials with different Cd/Mn ratios. The as-prepared spinels are slightly understoichiometric in the oxygen content, but at appropriate *T* and $P(O_2)$ they became overstoichiometric. The electrical transport takes place by motion of electron holes that are created by oxygen overstoichiometry at low *T*. At higher temperatures a different conduction mechanism is active. This mechanism is likely related to the thermal promotion of electrons from the valence into the conduction band. © 2000 Academic Press

1. INTRODUCTION

$CdMn_2O_4$ is a promising material for electrochemical (potentiometric) sensors of oxygenic gases (NO_x) in high-temperature detection of combustion exhausts (1–3). The working principle of these sensors (1–3) may be thought of as being based on two reactions,

$$2NO_2 + 4e^- \rightarrow 2NO + 2O^{2-} \quad [1]$$

and

$$O_2 + 4e^- \rightarrow 2O^{2-}, \quad [2]$$

taking place simultaneously (opposite to each other) at the sensing electrode, thus determining its mixed potential. The sensing electrode is typically connected to an O^{2-} conducting solid electrolyte (usually a stabilized zirconia layer), which acts also as a reference electrode.

[1]To whom correspondence should be addressed.

In a recent investigation we have shown that Cd/Mn spinels can be regarded as solid solutions between $CdMn_2O_4$ and Mn_3O_4. A material with a Cd stoichiometric coefficient lower than 2 can easily be prepared: in this case the Mn(II) enters the tetrahedral sites, thus producing a range of solid solutions that ideally require no vacancies in the tetrahedral sites nor oxygen vacancies (4). It is the aim of the present work to investigate the synthesis, structure, defect equilibria, and electrical properties of $CdMn_2O_4$ and related materials, and to gain the basic knowledge needed to provide a rational understanding of their promising applications.

2. EXPERIMENTAL

2.1. Materials

Several samples of cadmium manganese spinel with different cadmium contents were prepared as reported in the results section, following different synthetic paths. In particular $Cd(NO_3)_2 \cdot 4H_2O$ (Aldrich, 98%) and $Mn(NO_3)_2 \cdot nH_2O$ (Aldrich, 98%) were used for the sol–gel trials, while CdO (Aldrich, 99.5%) and Mn_2O_3 (Aldrich, 99%) were used for the solid state syntheses.

2.2. Instruments and Methods

X-ray powder diffraction patterns were acquired on a Philips 1710 diffractometer operated at 40 keV and 35 mA and equipped with a Cu radiation tube, adjustable divergence slit, graphite monochromator on the diffracted beam, and proportional detector. The lattice constants were determined by minimizing the weighted square difference between calculated and experimental Q_i values, where $Q_i = 4 \sin^2 \theta_i / \lambda_i^2$; weight $= \sin(2\theta_i)^{-2}$. Instrumental aberrations were considered by inserting additional terms in the linear least-squares model (5). SEM and EMPA inspections were performed with a JEOL JXA-840 A scanning electron microscope. A Zeiss Axioplan was used for optical microscopic inspections. Thermogravimetric and isothermal

0022-4596/00 $35.00

gravimetric measurements were performed under different atmospheres (obtained by flowing into the apparatus certified mixtures of oxygen in nitrogen) with a TA 2000 thermal analysis system, equipped with a TA 951 thermogravimetric analyzer. Electrochemical experiments were executed in a home-made apparatus which permits measurements to be taken up to 1000°C and under selected atmospheres. Impedance Spectroscopy (IS) measurements were carried out by means of a Solartron 1170 frequency response analyzer, equipped with an active guard for minimizing noise and capacitive effects of cables (6). For the measurements, samples were prepared in the form of cylindrical pellets and platinum electrodes were sputtered on the flat surfaces. DC conductivity measurements were performed by means of a Solartron 1286 galvanostat and a Keithley 180 digital nanovoltmeter, using the four-probe method, on samples shaped in the form of parallelepipeds.

3. RESULTS

Two synthetic paths to $CdMn_2O_4$ have been investigated: the coprecipitation technique and solid state reaction.

We have tried to apply the same coprecipitation route that was found to be effective for Ni/Mn spinels (7, 8). Therefore, excess oxalic acid was added to an ethanol solution of stoichiometric amounts of Cd and Mn(II) nitrates. The obtained precipitate was then heated at 300°C for a total amount of 5 hours. Powder diffraction analysis of the reaction mixture showed that this procedure mainly gives CdO and Mn_3O_4 with a poor fraction of the desired spinel, and that to complete the reaction repeated heating cycles to 750°C are required. A second trial with this method was done using coprecipitation of the hydroxides and carbonates from aqueous solutions. With heating at 300°C the hydroxides yielded CdO and Mn_2O_3 with a larger amount of the desired compound, while with heating at the same temperature the carbonates gave CdO and $Cd_2Mn_3O_8$. In both cases completing the reaction was found to be even more difficult than starting from oxalates.

The above-reported results imply that the completion of the coprecipitation route in the case of $CdMn_2O_4$ requires a solid state reaction between CdO and Mn_2O_3. We therefore explored directly the solid state reaction. Problems concerning the toxicity of CdO, and its remarkable vapor pressure, were addressed by using a closed reaction environment. The synthetic procedure is as follows: appropriate amounts of CdO and Mn_2O_3 powders were vigorously stirred in a solvent (acetone or isopropanol), until a complete solvent evaporation was obtained. The mechanical mixture was then isostatically pressed into a pellet, dried overnight at 200°C under vacuum, sealed in a quartz ampoule under vacuum, and allowed to react at 800°C in a controlled furnace.

Eight days with repeated regrinding and repelletization steps were necessary to achieve complete dissolution of the parent oxides into the spinel structure. The single-phase nature of the material so produced was assessed by X-ray powder diffraction, as shown in Fig. 1. Inspections of the powder morphology with optical and SEM microscopy, and electron microprobe analysis (EMPA), showed that the cation distribution is very homogeneous. Various mixed oxide samples were prepared with different Cd/Mn ratios starting from different CdO/Mn_2O_3 amounts. As a matter of fact, the Cd/Mn ratio of the final products (as measured with EMPA) is always somewhat lower than the corresponding ratio of the starting powder mixtures: this can be attributed to the sublimation of CdO during the prolonged firing at high temperature, which is not avoided, but just limited by the use of a closed quartz ampoule. In addition, we cannot exclude a reaction of the CdO vapor with the SiO_2 of the ampoule. In any case, every sample was found by EMPA to be very homogeneous in the cation distribution.

As it was previously stated, in a recent investigation (4) we have given direct XAS evidence that Mn actually enters tetrahedral sites of the spinel structure, and that the mean oxidation state of Mn smoothly changes from $CdMn_2O_4$ (only Mn^{III}) to Mn_3O_4 (which can be written as $Mn^{II}Mn^{III}_2O_4$). Therefore, $(Cd_{1-x}Mn^{II}_x)^t[Mn^{III}]^o_2O_4$ is a convenient formula for describing the present materials; the superscripts t and o refer to the tetrahedral and octahedral sites of the spinel structure. The x values of the various samples, as obtained by EMPA determinations, are 0.27, 0.17, 0.13, 0.11, 0.08, and 0.04. These are mean values of at least 10 analyses for each sample, made at different points, and with a standard deviation that is always lower than 1%, which confirms the very homogeneous cation distribution of the prepared samples. According to our previous experience, a reasonable estimate of the global analytical error in the determination of x is ± 0.03.

In all cases, the powder patterns can be indexed in agreement with the tetragonally distorted spinel structure with "normal" cation arrangement reported by Sinha *et al.* (9) for stoichiometric $CdMn_2O_4$. The regular trend of the lattice constants (see Fig. 2), the comparison of the individual patterns, the lack of diffraction peaks other than those of the $CdMn_2O_4$ spinel structure, and the very homogeneous cation distribution found by EMPA strongly indicate that the present samples actually correspond to a broad range solid solutions based on the regular $CdMn_2O_4$ structure.

The thermal stability of the $(Cd_{1-x}Mn^{II}_x)^t[Mn^{III}]^o_2O_4$ samples has been studied by means of thermogravimetry. The data hereafter reported refer to a $(Cd_{0.9}Mn^{II}_{0.1})^t[Mn^{III}]^o_2O_4$ sample, but the same behavior can be detected for all the samples. Heating the sample in pure oxygen flux up to 700°C causes a small weight increase which amounts to 1%, as shown in Fig. 3. This first weight

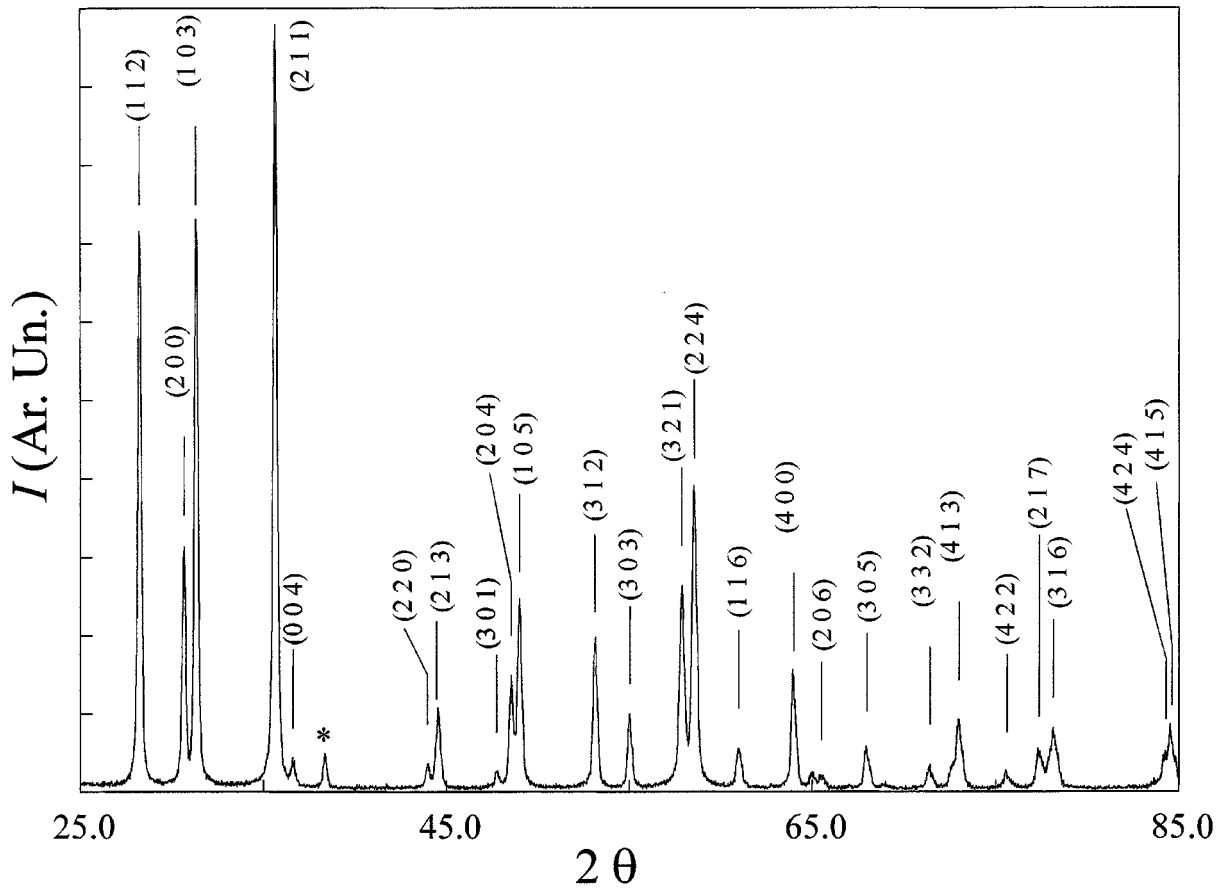

FIG. 1. XRPD patterns of the material obtained after the solid state synthesis procedure. The indexing refer to the tetragonal spinel structure of $CdMn_2O_4$. The peak marked with an asterisk is due to the Al sample holder. This sample corresponds to $x = 0.08$ in $(Cd_{1-x}Mn^{II}_x)^t[Mn^{III}]^o_2O_4$.

increase is irreversible: we tentatively assign it to a slight oxygen understoichiometry of the starting samples with respect to their equilibrium oxygen content. It may be helpful to reiterate here that the samples are prepared in a vacuum. During the following cooling steps, the samples gain further weight, as also shown in Fig. 3. This latter behavior is clearly reversible, as it is well reproducible during successive heating or cooling steps. The much smaller increase on cooling (or decrease on heating) is due to a small variation of *equilibrium* oxygen stoichiometry with temperature.

Due to the very small deviation of the oxygen content from the stoichiometric value of 4, absolute values of oxygen nonstoichiometry of the various samples were extremely difficult to obtain: we get some indication of a slight oxygen overstoichiometry. Isothermal relative variations of the oxygen content upon changing the equilibrium oxygen partial pressure, though small, are much more reliable. For $(Cd_{0.96}Mn^{II}_{0.04})^t[Mn^{III}]^o_2O_{4+\delta}$ we have found that the variation of δ $\Delta\delta$ is 0.018 at 500°C and 0.012 at 700°C when the equilibrium oxygen partial pressure is changed from 1 to 10^{-2} atm.

Charge transport measurements were performed on a $(Cd_{0.9}Mn^{II}_{0.1})^t[Mn^{III}]^o_2O_4$ sample. We started using impedance spectroscopy (IS) to assess the contributions of different mechanisms. Figure 4, in particular, shows the results at 200°C in air. The presence of a single semicircle leads to the conclusion that there is no grain boundary conductivity and that it is safe to assign the charge transport entirely to bulk contributions. Figure 5 compares IS determinations of conductivity (from nonlinear least-squares fitting of the frequency scan data) with the four-electrode direct current determinations. The same figure also compares the same kind of determination on the same sample after a long time delay (6 months), thus showing the excellent long-term stability of the electrical properties. This comparison is a direct confirmation of the reliability of IS for measuring the electrical properties of a material: it is apparent that neither (a) geometrical factors related to the sample shape nor (b) the possibility of differences induced by the different current regimes plays an important role in this kind of measurement.

It should be noticed that the above-reported small variations in the oxygen content in a semiconducting oxide such

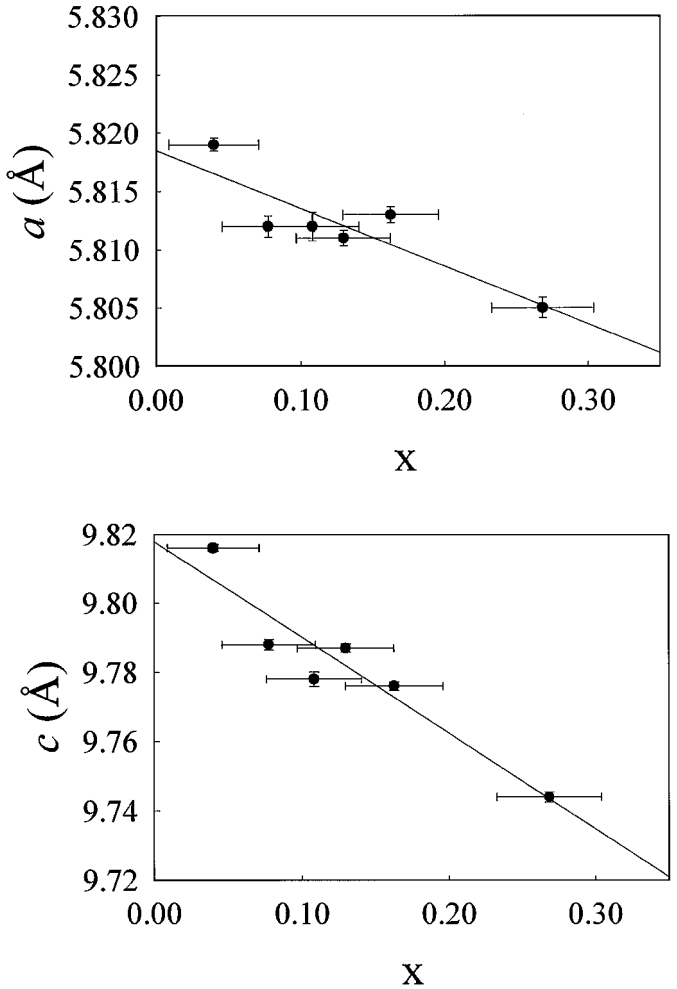

FIG. 2. Lattice constants in $(Cd_{1-x}Mn^{II}_x)^t[Mn^{III}]^o_2O_4$ as a function of x.

as $(Cd_{0.9}Mn^{II}_{0.1})^t[Mn^{III}]^o_2O_{4+\delta}$ can have a quite remarkable effect on the charge transport properties. We have therefore further investigated this point by performing conductivity

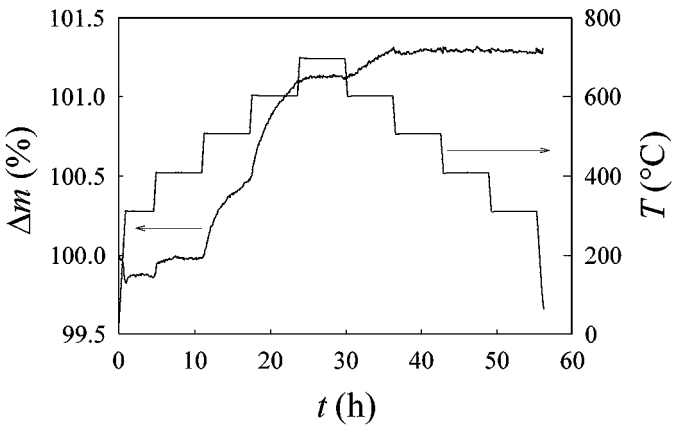

FIG. 3. TG curve for a $(Cd_{0.9}Mn^{II}_{0.1})^t[Mn^{III}]^o_2O_4$ sample in pure oxygen flux.

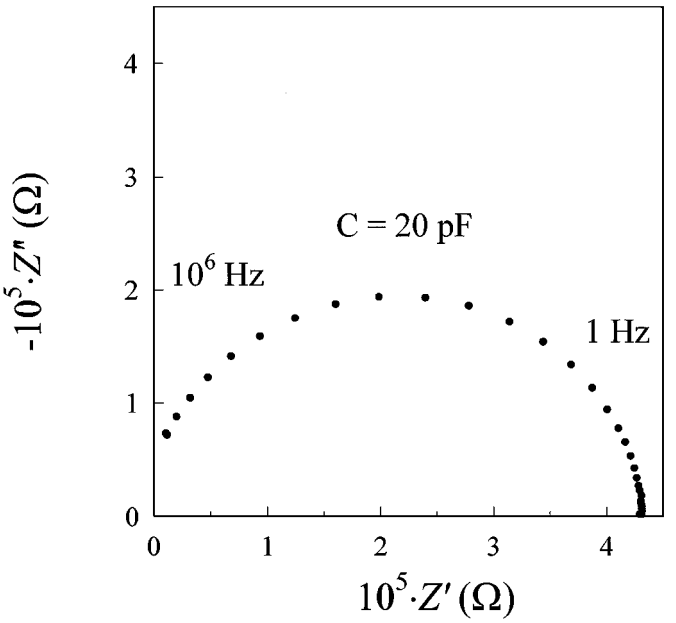

FIG. 4. IS data for a $(Cd_{0.9}Mn^{II}_{0.1})^t[Mn^{III}]^o_2O_4$ sample at 200°C in air.

measurements at different oxygen partial pressures, as shown in Fig. 6, where these data are plotted as a function of $1/T$ (Arrhenius plots). The transition from a transport

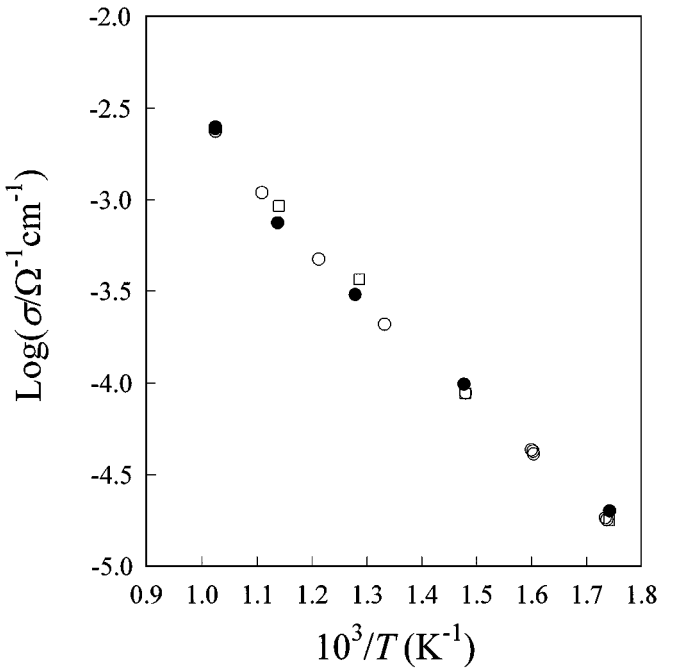

FIG. 5. Comparison of conductivity data for a $(Cd_{0.9}Mn^{II}_{0.1})^t[Mn^{III}]^o_2O_4$ sample at different temperatures in pure oxygen, obtained from IS and DC conductivity measurements. White squares, IS data on the freshly prepared sample; white squares, IS data on the same sample 6 months later; black circles, DC data.

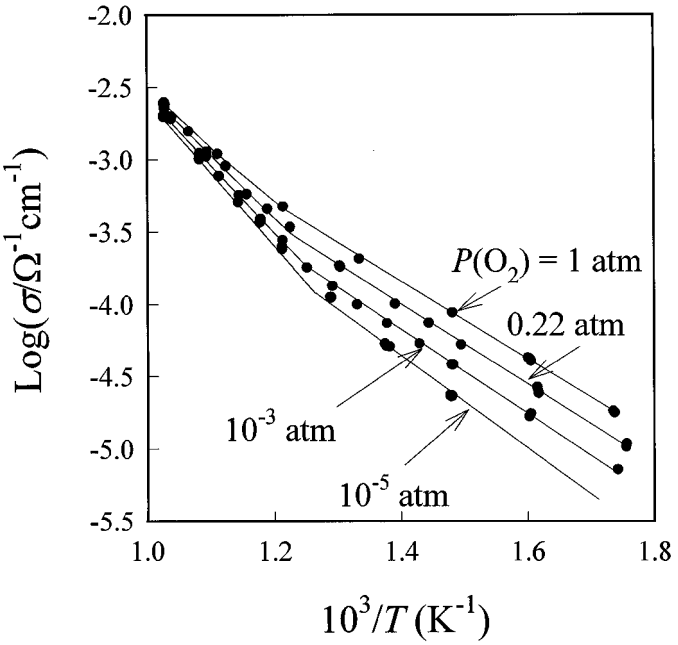

FIG. 6. Arrhenius plots for conductivity for $(Cd_{0.9}Mn^{II}_{0.1})^t[Mn^{III}]^o_2O_4$ at different oxygen partial pressures.

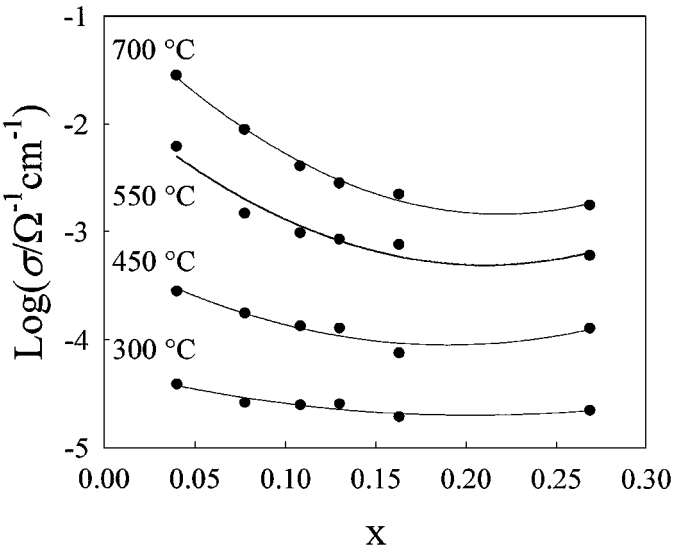

FIG. 8. Dependence of conductivity on x in $(Cd_{1-x}Mn^{II}_x)^t[Mn^{III}]^o_2O_4$ at different temperatures.

regime controlled by oxygen partial pressure to a nearly $P(O_2)$-independent regime can easily be seen, and corresponds to a change of the apparent activation energy from 0.4 eV (low-temperature range) to 1.1 eV (high-temperature range). The same data are reported as a function of $P(O_2)$ between 300 and 700°C in Fig. 7. When plotted on a logarithmic scale, the experimental data at the lowest investigated temperature show a good linear trend with a slope near 1/6.

Finally, Fig. 8 shows how the electrical conductivity (at $P(O_2) = 1$ atm and $300 < T < 700$°C) changes with the Cd/Mn content of the samples.

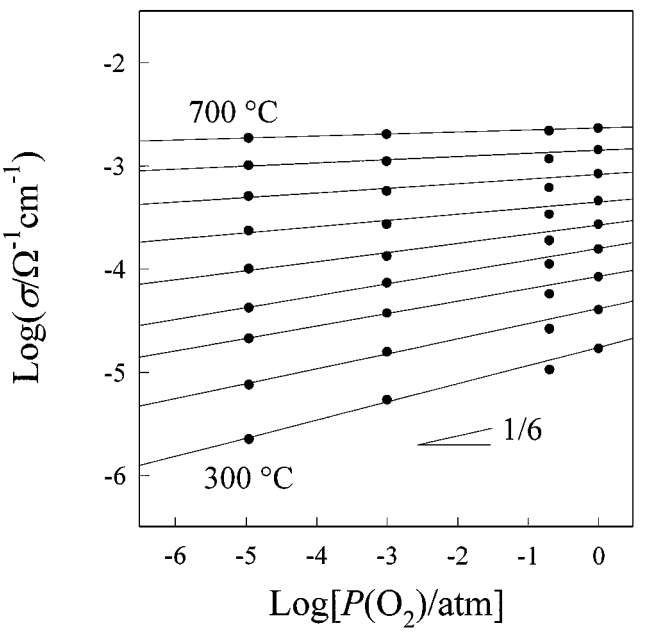

FIG. 7. Conductivity of $(Cd_{0.9}Mn^{II}_{0.1})^t[Mn^{III}]^o_2O_4$ as a function of the oxygen partial pressure. The data are obtained at different temperatures between 300°C and 700°C with increments of 50°C.

4. DISCUSSION AND CONCLUSIONS

With solid state reaction of the parent oxides in a sealed quartz ampoule at 800°C it is possible to synthesize mixed oxides with different Cd/Mn ratios.

These materials are single phase and belong to the spinel structure of stoichiometric $CdMn_2O_4$. Sinha *et al.* (9) have shown that the same basic structural features ("normal" cation arrangement and tetragonal distortion of the $Mn^{III}O_6$ octahedron with the apical oxygens farther than the other ones) also characterizes Mn_3O_4, where Mn^{II} replaces Cd in the tetrahedral sites. This fact and the regular trends of lattice constants and X-pattern line intensities of samples with various Cd/Mn ratios in the investigated range are strongly indicative of broad range solid solutions based on the regular $CdMn_2O_4$ structure with variable amounts of Mn substitutions on the Cd sites.

Under equilibrium conditions, the various defects of the above-referenced structure are controlled by three external variables, Cd/Mn content (cation molecularity), oxygen potential (or oxygen stoichiometry), and temperature, and are described by several equilibrium equations. The experimental results can be used to simplify the treatment and

reach a reliable approximate description. Generally, the majority defects in spinels are cation vacancies. The main quasichemical equilibrium for oxygen nonstoichiometry must therefore be written as

$$2O_2(\text{gas}) \rightleftarrows 4O_O^x + V''_{Te} + 2V'''_{Oc} + 8h^\bullet$$

where the subscripts Oc, Te, and O denote octahedral and tetrahedral (cation), and oxygen sites, respectively. Predominance of this equilibrium gives rise to (a) oxygen overstoichiometry, (b) semiconductor (*p*-type) electrical conductivity (σ), and (c) a power-law dependence on oxygen partial pressure,

$$\sigma = \mu(h^\bullet)e[h^\bullet] \propto P(O_2)^{2/11}$$

where $\mu(h^\bullet)$ is the hole mobility, square brackets denote concentration, e is the (positive) elementary charge, and the last relation comes from the solution of the equilibrium equation coupled with charge and site balances.

This behavior is actually in agreement with our experimental results. As said, our thermogravimetric data are in favor of an oxygen content above the stoichiometric value of 4. A thermally activated electrical conductivity is well assessed by the Arrhenius plots, while the logarithmic plots of conductivity against oxygen partial pressure show at low T a slope quite close to the expected value of $+2/11$, which is also an indication of hole conductivity.

The different (higher) activation energy for conductivity at high temperatures and its independence from oxygen partial pressure mark the transition to predominance of a different defect equilibrium, which is very reasonably due to the direct intergap ionization to an electron–hole couple,

$$\text{nil} \rightleftarrows e' + h^\bullet$$

with a band gap around 2.2 eV. This second mechanism prevails at high temperatures, when one can assume that the oxygen content becomes nearly independent of the oxygen partial pressure: this assumption is nicely substantiated by the very small value of the variation in the oxygen content we have found at 700°C (0.012) when the equilibrium oxygen partial pressure is changed from 1 to 10^{-2} atm.

Finally, the increasing conductivity in $(Cd_{1-x}Mn_x^{II})^t[Mn^{III}]_2^oO_4$ with increasing Cd content is possibly related to some form of hole localization on Mn^{II} occurring in the Mn-rich materials. The discussion of the reasons why this hole localization should take place is far beyond the aims of this paper. At this point, this should be regarded as a reasonable rationale that needs further investigation.

ACKNOWLEDGMENTS

This work has been partially supported by Progetto Finalizzato MSTA II.

REFERENCES

1. N. Yamazoe and N. Miura, *Solid State Ionics* **86–88,** 987 (1996).
2. N. Miura, G. Lu, N. Yamazoe, H. Kurosawa, and M. Hasei, *J. Electrochem. Soc.* **143,** L33 (1996).
3. N. Miura, H. Kurosawa, H. Hasei, G. Lu, and N. Yamazoe, *Solid State Ionics* **86–88,** 1069 (1996).
4. P. Ghigna, G. Flor, and G. Spinolo, *J. Solid State Chem.* **149,** 252 (2000).
5. G. Spinolo and F. Maglia, *Powder Diffraction* **14,** 208 (1999).
6. G. Chiodelli and P. Lupotto, *J. Electrochem. Soc.* **138,** 2703 (1991).
7. B. Gillot, J. Baudur, F. Bouree, R. Legros, and A. Rousset, *Solid State Ionics* **58,** 155 (1992).
8. C. Laberty, J. Pielaszek, P. Alphonse, and A. Rousset, *Solid State Ionics* **110,** 293 (1998).
9. A. P. B. Sinha, N. R. Sanjana, and A. B. Biswas, *Acta Crystallogr.* **10,** 439 (1957).